Journal of Information Systems Engineering and Management
2025, 10(37s)
e-ISSN: 2468-4376
https://www.jisem-journal.com/

Research Article

Adaptive and Extensive Classification for Optimal Multi-Feature Selection on Covid's Data

R. Ashok Kumar[1], Shaheda Akthar[2]
[1] *Research Scholar, Dept. of CSE, Acharya Nagarjuna University, Guntur, AP & Lecturer in Computer Science, SCIM Government College (A), Tanuku, West Godavari, AP, India*
[2] *Dr. Shaheda Akthar, Lecturer in Computer Science, Government College for Women (A), Guntur & Research Supervisor, Dept. of CSE, Acharya Nagarjuna University, Guntur, AP*

ARTICLEINFO

Received: 29 Dec 2024

Revised: 12 Feb 2025

Accepted: 27 Feb 2025

ABSTRACT

Coronavirus (CD) is a disease that impacts the brain's motor system. Tremors, muscular rigidity, inaccurate gait, and speech difficulty are the hallmarks of CD. A definitive diagnosis of Covid's disease generally requires multiple neurological, psychological, and physical examinations, even though the main symptoms cannot be readily distinguished from those of other disorders. This has led to a number of recent initiatives to use machine learning-based automated diagnostic assistance systems to better assess CD patients. Automatic early identification of COVID-19 using feature data sets is one of the most difficult medical problems that exist today. Some features of these datasets are useless, and others are rife with problems like noise that make learning difficult and increase the amount of computing power needed. To improve the efficiency of feature selection and guarantee the classifier's most accurate performance. Implement a Novel Stacked Convolutional Neural Network Model (NSCNNM) in this study to automatically diagnose COVID-19 illness.Our objective is to develop a system, which can accurately detect and categorize COVID-19 using chest radiographs and is based on deep learning. We begin by contrasting the efficiency of different cutting-edge convolutional neural networks (CNNs) suggested for medical picture categorization in the past few years. Second, when building and developing CNN, we begin at the very beginning. In both situations, we train and validate with the publicly accessible X-Ray dataset. We accomplished the tertiary classification task (Normal/COVID-19/Pneumonia) with 87.50% correctness and the binary classification task (Normal/COVID-19) with 98.33% accuracy by means of transfer learning. The CNN that was trained from the ground up achieves an accuracy of 93.75 percent when it comes to tertiary classification. The accuracy of classification using transfer learning drops as the number of classes grows. The results are shown by a 10-fold cross-validation confusion metric study and comprehensive receiver operating characteristics (ROC) analysis.

Keywords: *Convolutional Neural Networks (CNNs), Covid-19, Random Forest, Multiclass Classification, and Feature Selection*.

1. INTRODUCTION

The COVID-19 virus was initially identified in Wuhan, China, by the close of December 2019. Its source is still unknown. Ever since then, it has gone global in an instant.1e3 After six months, the majority of China had contracted the virus.4 on 11th Feb, 2020, WHO formally classified this specific virus-borne sickness as COVID-19.2 The initial COVID-19 report was received by Iran on February 21, 2020. Worldwide, 192 million cases have been found as of July 20, 2021, with approximately 3.5 million instances confirmed in Iran. The majority of coronaviruses infect animals, but because they are so prevalent, they can also infect humans. Humans contract severe acute respiratory sickness and death as a result of coronaviruses, specifically SARS-CoV.5 Coronavirus infections often manifest with fever, hacking coughing, throat pain, and headaches, dizziness, tiredness, muscular pains, and trouble breathing.[6] Since its inception, the COVID-19 virulent disease has had a terrible impact on people healthiness, community welfare, businesses, and social ties. Relationships within families and participation in sporting activities have also taken a hit, as has the standard of education at colleges and universities.

As far as human COVID-19 diagnosis goes, the RT-PCR test stands head and shoulders above the rest. It takes a long time to identify something using this procedure, and there's a good chance that it will be false negatives. However, X-rays and Computed Tomography (CT) scan of the chest are helpful in detecting and treating this illness

early on, especially in pregnant women and small children. When diagnosing chest pathology, chest X-ray radiographs (CXRs) are frequently employed, however when identifying COVID-19, they are not (9, 10).

Extensive research on CNN has been conducted in COVID-19 detection and classification [8, 9], with results that far outstrip those of earlier image recognition methods [10]. In general, CNN has shown that healthcare systems are incredibly capable in identifying those who are more likely to get sick.Binary and multi-class categorization is two examples of CNN's many possible uses.

The complex structures in high-dimensional datasets can already be effectively discovered using CNNs equipped with multi-layer function representations.The problem of how to discover COVID-19 quickly while using little data and achieving high classification accuracy remains unsolved. When developing a detection system, it is crucial to consider both the amount of training data and its quality in terms of annotations. The studies shown in Figure 1 do not include any chest x-ray images from the openly accessible dataset. Because of the inadequate amount of COVID-19 data sample, transfer learning is preferred an effective classification method. To maximize accuracy with a small dataset, transfer learning involves taking learnt parameters from one task and applying them to another. The promising outcomes of transfer learning have demonstrated the efficiency of DL network in binary categorization [11]. We conducted several studies to determine how well the model could diagnose COVID-19.

• In two classification situations, we offer CNNs (VGG16, InceptionV3, Xception) based models for transfer learning. Involve normal/COVID-19 classification, while Scenario II involves normal/COVID-19/pneumonia classification.

To boost performance accuracy, we have suggested an innovative schema for scenario classification using a five-layer CNN.

• The outcomes of our experiments show that models work well in classification settings and have promise for detecting, controlling, preventing, and classifying COVID-19.

2. BACKGROUND WORK

Several computer-assisted approaches have been developed in the past four decades to aid in the analysis of lung disease [16], and some of such systems have showed promise in automatically identifying lung abnormalities from radiological images [17, 18]. Recent years have been a surge in interest in the automatically CAD of COVID-19 using radiological images, prompting publication of many methods in the field. They showcased the CAD system meant for COVID-19 identification with radiological imagery in multiple research studies [19, 20]. To identify CT scans as COVID-19, influenza virus pneumonia, or no infectivity, Xu et al. [21] performed a technical examination of multiple CNN models and then constructed a model that incorporates 2D and 3D CNN models. A specificity of 92.2% and a sensitivity of 98.2% were achieved by their approach. In order to separate CT scan images into those containing COVID-19 and those without, Shah et al. [22] developed a CTnet-10 model. In addition, they evaluated DenseNet-169, VGG-16, ResNet-50, Inception-V3, and VGG-19, among other pre-trained CNN networks, for COVID-19 detection. Studies discovered that the VGG19 model had the highest accurate rate of 94.52%. Kassania et al. [23] used a similar strategy to extract characteristics from X-ray and CT scans by combining various CNN models. Several machine learning classifiers were employed to sort the imagery into healthy and COVID-19 category using the retrieved features. Using DenseNet121 features, they asserted that the Bagging tree classifier obtained the greatest categorization accuracy at 99.00%.

For automatically identify COVID-19 in CT scans, Han et al. [24] introduced an attention-based deep 3D multi instances learning-based approach. This approach had a 97.9% success rate. In order to divide X-ray imagery into 4 groups—normal, bacterial, non-COVID, and COVID-19—Afshar et al. [25] developed a structure based on capsule-based networks. The sensitivity was 90% and the accuracy was 95.7% according to the authors. Ardakani et al. [26] stated a deep learning approach to COVID-19 recognition from CT scan imagery, and they examined 10 CNN models that had been pre-trained to see which one performed the best. The outcomes show that ResNet101 has the highest region below the curve (AUC) of any pretrained network at 0.99. Benmalek et al. [7] utilized three pre-trained convolutional neural network models—Resnet-18, Inception-V3, and MobileNet-V2—to investigate the accuracy of CT scan and X-ray imagery in diagnosing COVID-19 illness. Their top sensitivity for CT scans was 98.6% using ResNet-18, while for X-ray photos, it was 92.3% using Inception-V3. Using the VGG16 and ResNet50 frameworks, Mishra et al. [27] developed a transfer learning system to detect COVID-19 using CT scan imagery.

Journal of Information Systems Engineering and Management
2025, 10(37s)
e-ISSN: 2468-4376
https://www.jisem-journal.com/

Research Article

Their suggested strategy resulted in multi-class classification accurateness of 88.52% using ResNet50 and a binary classification accuracy of 99% with VGG16 and ResNet50 models combined.

In the same way, vein, Narin et al. [28] classified X-ray imagery into Normal and COVID-19 category using ResNet50, Inception-V3, and Inception-ResNet-V2 trained through transfer learning. With an accuracy rate of 98%, this method has shown good performance for ResNet50. Having said that, the quantity of 100 X-ray images is severely inadequate for the purpose of developing deep learning models. Using image patches obtained through chest X-ray imagery., Oh et al. [29] suggested a patch strategy for training the ResNet18 framework. They reached a decision-making accuracy rate of 88.9% by using the majority vote approach. A DarkCovidNet model based on objection detection was introduced by Ozturk et al. [30] for the purpose of automatically identifying COVID-19 from X-ray imagery. Those achieved a stated accurateness of 98.08 % in binary X-ray imagery classification as COVID-19 and no discoveries. When they used their method to multi-class X-ray imagery into pneumonia, no-findings, and COVID-19, the accuracy reached 87.02%. The following is a description of the x-ray of a COVID image:

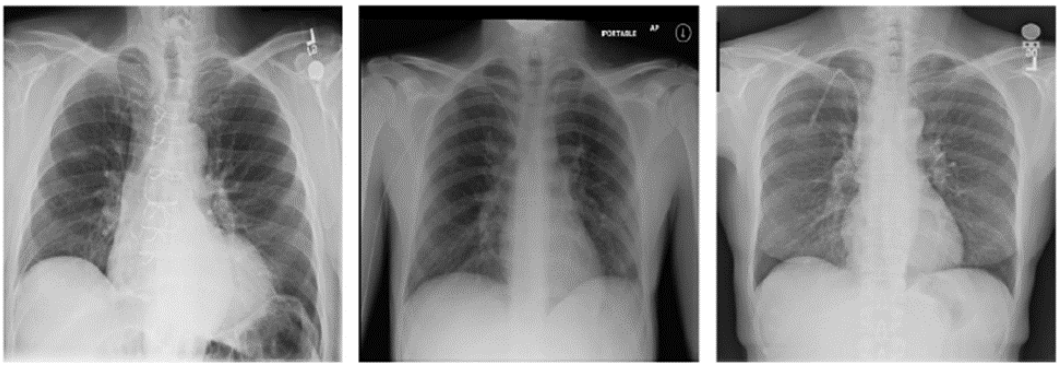

Figure 1 Image representation of human with x-ray formation.

In their hierarchical classification strategy, Pereira et al. [31] investigated texture descriptors and used Inception-V3 to extract deep features. They looked at fusion methods, both early and late, to combine the power of classifiers and descriptors. Their hierarchical classification model can identify COVID-19 in X-ray imagery with an F1-Score of 0.89. Sethy et al. [32] used a pre trained convolution neural network (CNN) to obtain deep features, which they subsequently loaded to support vector machine (SVM) for X-ray imagery categorization. The authors attained an accurateness of 95.38% with ResNet50 and the SVM classifier.

By utilizing COVID-19 chest X-ray imagery to refine four pretrained networks, Minaeet al. [33] suggested a similar transfer learning-based approach. Reportedly, the sensitivity rate was 98%. A set of ten pre-trained CNNs make up the ensemble-based model proposed by Castiglioni et al. [34]. An 80% sensitivity was achieved using their proposed strategy. Abraham et al. [35] used a CFS method with many pretrained CNNs to determine characteristics from the X-ray imagery. After deriving characteristics, the authors applied a Bayesnet classifier to identify COVID-19. With an accurateness of 91.16 %, their proposed approach correctly classified X-ray imagery into COVID-19 and non-COVID categories. Panwar et al. [36] proposed a nCOVnet model that uses deep learning to detect COVID-19 cases in X-ray images. They claimed accurateness rate for classification is 88.10%. In their work, Nigam et al. [37] utilized pretrained CNN architectures such as VGG16, DenseNet121, Xception, NASNet, and EfficientNet-B7 to establish a framework for diagnosing corona virus infections. According to the authors, EfficientNet-B7 can categorize chest X-ray imagery like normal, COVID, and other categories with an accuracy rate of 93.48 percent.

For the purpose of classifying chest X-ray imagery into normal and COVID-19 categories, Ashour et al. [38] suggested an ensemble-based bag-of-features (BoF) framework. Key points were identified using the grid approach, and robust features (SURF) were extracted from the image more quickly. With their suggested model, the classification accuracy was 98.6%.

3. BASIC PRILIMINARIES

We discussed before the challenge of creating a large-scale multiclass medical data classification system. Feature selection and rating, which are part of data preparation, are the perfect final steps to complete the classification

Journal of Information Systems Engineering and Management
2025, 10(37s)
e-ISSN: 2468-4376
https://www.jisem-journal.com/

Research Article

process. The feature selection technique eliminates irrelevant features in order to find the optimal ones [5]. This research made use of Information Gain, Gain Ratio, and Correlation as its three characteristic selection strategy. Feature selection approaches use ranking scores to get the required features. A popular metric for system unpredictability in information theory is entropy. One way to determine the entropy of is to use (1).

The formula H(y)"="-∑_(y∈Y)"This is the formula: p(y)log_"2" (p(y)). (1) y= from 1 to 1 represents the variable's marginal probability density function, P(y).The following step is to partition the training dataset's S values according to x's properties. The features y and x partition at the point where the entropy of the partitioned set (x) is less than the entropy of the complete set before partitioning (y). Then it would be clear that entropy x of is
the function H(y|x)"="-∑_(x∈X)"*(p(x)) = sum_(y∈Y)The logarithm of the inequality p(y|x) (〖p(y|x)〗) You can find the conditional probability of y given x in (2) by calculating p(y|x).

3.1. Information gain (IG)

The training set S is subjected to an impurity process known as entropy. It is the amount of additional information found in y after a decrease in entropy y, as measured by x. The full concept, is called as Information Gain (IG), is illustrated by (3).

This is the equation for the integral: "IG=H(" y")"-H(x|y)=H(" x")"-"H("(x|y) (3)
(3) Makes it extremely evident that the information retained after taking notes x and the information remembered during observation y are rather similar. If the features have many values and are not more biased and informative than the features generated by the criteria. This thus serves as the standard for a lack of. Similarly, for any feature function "f" _"m" = "F=" {"f" _"1" ","..〖",f" 〗_"M" }, we can apply (4) to obtain the information gain if the discretization cardinality of the function is equal to.
"IG" ** "B" ** "f" ** "m")"=" "I" ** "C|f" ** "m")/(**"log" **"2" "Γ") (4)
We may deduce from (4) that "I(C|f" 〗_"m" ")" is the information gain associated with "f" _"m" and "Γ" is the penalty for the information gain if and only if is the class variable.

3.2: The Gain Ratio (GR)

To address the issue of bias caused by information gain, an improved feature selection method known as gain ratio is employed. Additionally, it is compatible with the approach. The information gain metric "F" _"ei" related to the entropy in situation "GR" of is denoted by "GR" (5), as shown below.

The output is: "GR(C,F)_"ei" ")=" [("H" ("C")-"H" (〖"C|F" 〗_"ei"))/"H" ("F" _"ei") (5)

"H(C)" indicates the class entropy of "C," "H(C|F" 〗_"ei" ")" indicates the class entropy of "C" with respect to the features "F" 〗_"ei," and at last, "H(F" 〗_"ei" ")" is taken the "F" 〗ei" entropy of measure, as explained in (5)..

4. IMPLEMENTED METHODS

Through the use of empirical evaluation of classification improvement methodologies, this research aims to determine the efficacy of automated COVID-19 discovery using chest x-ray pictures. Two x-ray dataset sources were used in an experiment. This research aims to address the following related objectives:
• Efficiently classifying COVID-19 utilizing a chest x-ray by constructing a solid framework.
• Combine the proposed CNN with three pre-trained models to classify chest x-ray images.
The models' performance should be assessed and compared using performance measures.

4.1.Collection of Data

Images of COVID-19 were initially obtained from the database detailed by Cohen et al. [38]. A set of x-ray pictures gathered from the work of Cohen et al.,” 26”. A total of 296 photos showcasing 83 female and 175 male COVID-19 positive individuals are included in the dataset. There is missing metadata for several patient details in this dataset. In addition, Kermany et al. [39] bacterial pneumonia x-ray pictures were acquired for the purpose of classifying COVID-19 and pneumonia. The experiment dataset was specifically created by merging and updating the two data repositories. There are a total of 1,341 healthy photos in the dataset, 296 images with confirmed or suspected cases

Journal of Information Systems Engineering and Management
2025, 10(37s)
e-ISSN: 2468-4376
https://www.jisem-journal.com/

Research Article

of COVID-19, and 3,875 images with confirmed cases of viral or bacterial pneumonia. Thus, it is possible to see data imbalance in the collected data displayed in Figure 3, which could lead to inaccurate categorization outcomes. So, we went through each shot by hand and cropped out the ones that were too dark or too light. A total of 140 photos were chosen for our experiments from each category.

4.2. Brain network with convolutional layers

When it comes to medical lesion diagnosis utilizing images, CNNs have recently been the most researched machine learning (ML) algorithm [40]. This is because, when processing incoming images, CNNs manage to hold on to complicated features. As mentioned before, the main focus of radiology is on spatial relationships, such as the joint between bone and muscle or the interface between normal lung tissue and diseased cells. In Figure 4 we can see the system architecture, and in Table 1 we can see the chosen hyperparameters. The suggested CNN design incorporates five convolution layers that receive a 244 x 244 tensor image of the chest as input. After that, the first convolution layer makes use of 64 of these 5 × 5 × 3 kernel filters having a stride of 1 × 1. The results of the first layer are passed to subsequent max-pooling layer with a 2 × 2 stride, this compresses the input to fifty percent its initial dimension (112 × 112). Every layer uses the ReLU activation feature to process the results of the pooling layer. The nonlinear output that was previously acquired is now sent to the convolution layer through 128 filters and a 5 × 5 × 64 matrix, using the same 1 × 1 stride value. Once it has been processed via a max-pooling layer using the same 2 × 2 strides, the output is shrunk to 56 × 56, which is half of its initial size. After going through ReLU activation, the output is delivered to the 3rd convolution layer, it has 256 filters, a kernel dimension of 5 × 5 × 128 through a 1 x 1 stride. After the result is sent to a max-pooling layer, a tensor with dimensions of 28 × 28 is generated.

Following its activation by ReLU, the output is once again sent into the fourth convolution layer. This layer shares the same 1 × 1 stride, 512 filters, and 5 × 5 × 256 kernel size. The result of the 4th convolution is max-pooled to a size of 14 × 14. The data is forwarded to a 5th convolution layer through 512 filters and a 14 × 14 × 512 kernel dimension when ReLU is activated. All of the filters from the other levels can be handled by this one. The 14 × 14 output is obtained by max-pooling the result through this layer with a 2 × 2 stride. The tensor that is produced now has the shape 7 × 7 × 512. The generated tensor has become flat using 25088 neurons in total. The proximity of COVID-19 symptoms is shown by the weighted numbers that take the form of neurons. By removing values using the dropout layer, network overfitting can be addressed. Half of the participants in the trial dropped out during training. After reducing the tensor with 25088 neurons to 64 neurons in the fully linked layer, the output is improved via ReLU activation. There is a direct correlation between the number of retinal image category (Normal, COVID-19, and pneumonia) and number of neurons converted from the tensor with 64 neurons (the outcome of the fully linked layers).Convolutional layer: It is possible to locate the kernel and several filters in this layer. Each filter uses an intricate process that involves creating a new layer and applying it to the input image in order to extract features. Each layer highlights a different aspect of the supplied image. The symbol represents the convolution operation. Here we define F(t), the output or function map, when in(t) is convoluted with a filter or f(a) kernel.

$$F(t) = (I_n * f)(t)$$

This distinct convolution is given by the subsequent equation if t can only take integer values:

$$F(t) = \sum_a I_n(a) \cdot f(t-a)$$

So far, we have presumed that the convolutional process is one-dimensional. An operation that uses a kernel f(a, b) and input In(m, n) in two dimensions is called a convolution:

$$F(t) = \sum_a \sum_b I_n(a,b) \cdot f(m-a, n-b)$$

Because of the commutative law, we can invert the kernel and get:

$$F(t) = \sum_a \sum_b I_n(m-a, n-b) \cdot f(a,b)$$

Like convolution but without kernel reversal, cross – sectional function with applied neural networks

$$F(t) = \sum_a \sum_b I_n(m+a, n+b) \cdot f(a,b)$$

Journal of Information Systems Engineering and Management
2025, 10(37s)
e-ISSN: 2468-4376
https://www.jisem-journal.com/

Research Article

The ReLU layer is a rectified linear unit. This layer activates the mechanisms that zero the negative inputs value, which makes analysis, training faster, more efficient and assists to keep the gradient from fading. In mathematical terms, this is represented as:

$$R(x) = max(0, x)$$

When the neuron receives x as input.

In the maxpooling layer, a sample-based discretization technique is used. After compressing the dimensionality of an input structure (input imagery, hidden layers, output matrix, etc.) and down sampling it, approximations regarding the various elements accessible in the discarded smaller regions can be generated.. In addition to delivering crucial interpretative invariability to internal representation, this would further decrease computing expense by minimizing the quantity of learning parameters. A 3 × 3 kernel size was utilized by our model in the Max-pooling technique. Next, the last convolution block, the network collapsed to a single-dimensional state.

Making batches consistent. The network's layers are able to learn from each other in a relatively autonomous manner because of batch normalization. In addition to normalizing the result from the previous activation layer and divide the batch standard deviation by subtraction of the batch mean, it further strengthens the neural network.

Everything in this layer is linked. To find the probability values for grouping, the layer uses as input the outcomes of the Convolutional, ReLU, or Pooling layers that came before it.

Section 3.2.6 explains the loss function. Using a soft-max function, this layer processes the provided sampling of data. The final forecast involved the use of this layer. Therefore, our loss function is as follows:

$$L_i = -\log\left(\frac{e^{\beta_y}}{\sum_j^c e^{\beta_j}}\right)$$

The j^{th} component of the vector of class scores ŏ is represented by oj, and Hy is the CNN score for the positive class when c is the number of classes for every picture. The SoftMax assures that the logarithm of the equation accurately predicts the future.

The regularization process makes use of a dropout regularization method due to its efficiency. Srivastava et al. claimed that this strategy was being advocated. Keeping the neuron dynamic through a predefined likelihood P or set it to 0 is one technique to introduce dropout during training. The best regularized results are obtained with a hyper parameter of 0.50, which is why we use it here.

4.3. Learning of Transfer

In highly complex industries, a knowledge transfer through sources to intended tasks is sometimes the only practical choice because large-scale, high-quality data acquisition is so challenging. Not only is using pre-trained weights an efficient optimization method, but it also frequently helps with classification sensitivity. Common features like borders, textures, and patterns are learned by the first CNN layer. Alternatively, diseased lesions and other complex features are given greater attention in the higher layers of the image. Most networks, particularly those used for computer-aided diagnosis (CAD), have their top layer trained with the target dataset and their lower layers' parameters initialized. Not only does using fewer training parameters improve performance, but it also decreases the likelihood of over-fitting, a major problem with Neural Network training. Automatic COVID-19 identification makes use of convolutional neural networks (CNNs) trained using transfer learning, which are briefly described here. In this experiment, the TensorFlow back-end—which contains weights and pre- Keras Apps provides already trained DL models —and the Keras DL Framework—created by Chollet F—were both used. In this study, we followed the work of S. Pal. [46] and K. Simonyan [47] by using the VGG16, InceptionV3, and Xception models with pre-trained weights from the ImageNet database.

Over 3.2 million photos with detailed annotations over 5247 categories make up the ImageNet dataset, which is based on the hierarchical structure of WorldNet [48]. Therefore, the models that were used are detailed below. The

Journal of Information Systems Engineering and Management
2025, 10(37s)
e-ISSN: 2468-4376
https://www.jisem-journal.com/

Research Article

pre-trained VGG16 model has shown promising results after learning to extract picture features that can distinguish between distinct picture classes.

Table 1. Layer by layer evaluation of covid extraction from biomedical human image.

Layers	layer Type	Output Shape	Trainable parameters
1	Cov2d	[224, 224, 64]	1792
2	Cov2d	[224, 224, 64]	36928
4	Cov2d	[112, 112, 128]	73856
5	Cov2d	[112, 112, 128]	147585
6	Cov2d	[56, 56, 256]	295168
7	Cov2d	[56, 56, 256]	590080
8	Cov2d	[56, 56, 256]	590080
9	Cov2d	[56, 56, 256]	590080
10	Cov2d	[28, 28, 512]	1180160
11	Cov2d	[28, 28, 512]	2359808
12	Cov2d	[28, 28, 512]	2359808
13	Cov2d	[14, 14, 512]	2359808
14	Cov2d	[14, 14, 512]	2359808
15	Cov2d	[14, 14, 512]	2359808
16	Cov2d	[14, 14, 512]	2359808

One hundred forty-four million Deep Convolutional Neural Network (CNN) models, which are also called VGGNet, have sixteen convolution layers, each with a 3 × 3 deep visual field, 5 max-pooling layers, each with a 2 × 2 size, for spatial pooling, and lastly, 3 fully connected layers, with the soft-max layer serving as the last layer. The ReLu test was performed on all hidden layers. Furthermore, the model makes use of the regularization of dropouts in the fully connected layers. After eliminating the bottleneck layer—a fully connected classifier—from the already-trained VGG16 network, we may use it to generate semantic picture vectors. The classifier used was softmax, and the model was pre-trained with VGG16. In Table 1 you can observe the overall structure and parameters of VGG16. In chest x-ray images, it yielded remarkably precise findings

4.4. Implemented approach based on Learning of Transfer

Image preprocessing and the 2nd Learning Model are the two main components of the proposed approach. The morphological process was mostly used for preprocessing, while the deep transfer framework was utilized for train, validate, and testing. The provided model incorporates a group of transfer learning systems and is stated by \ ={VGG16, InceptionV3, Xception}. Y is a shared class with the formula Y = {y/y{Normal;COVID – 19;Pneumonia}}, and X is a collection of N data inputs with dimensions 224 × 224. This dataset is used to train the peak layer of all deep transfer models

A dataset was partitioned into two parts: a training set (trainx; trainy) that was used for training 80 percent of the time and a testing set that was used 20 percent of the time.

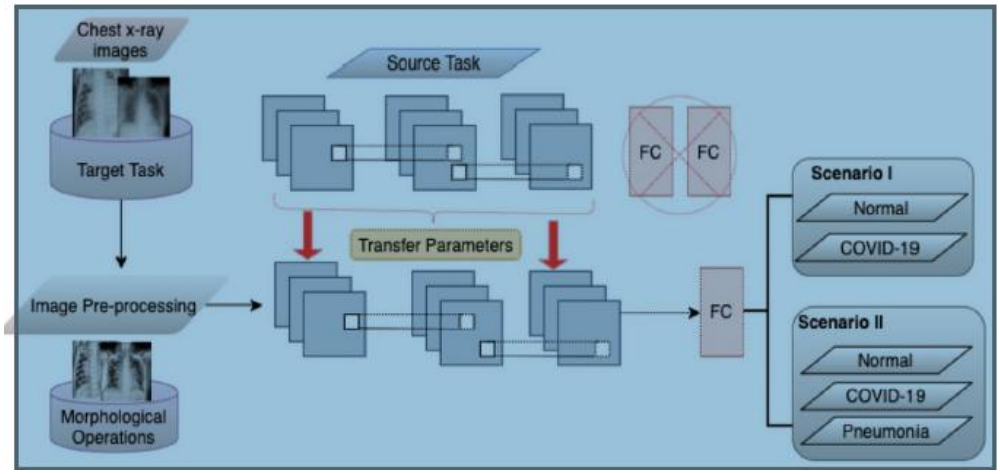

Figure 2 Implementation process to identification of Covid 19

Journal of Information Systems Engineering and Management
2025, 10(37s)
e-ISSN: 2468-4376
https://www.jisem-journal.com/

Research Article

A training-to-validation ratio of 80% has confirmed efficient in many domains. After the training data is separated into small batches of size n = 32, the CNN framework is optimized for minimizing functional loss using each small batch (Xi;Yi)(trainx;trainy) where i =1; 2; 3;..... ::;Nn. This is shown in equation 7 and 8, respectively, for categorical and binary cross entropy loss

$$L_b = -\sum_{i=1}^{i=2} t_i log(\beta_i) = -t_1 log(\beta_1) - (1 - t_1) log(1 - \beta_1)$$

Co contains two classes, c1 and c2, according to the statement. There is β1 and t[0, 1] for class c1. The true value for class c2 is t2 = 1 - t1 and β2 = 1 - β1.

Researchers used a large collection of ImageNet photos depicting a wide variety of objects—from cars and fruits to horses and more—to pre-train the study's categorization algorithms. Although the algorithms outperform other methods when trained on the object-based dataset, they are still limited to a small subset of industries, such as medical lesion detection. Chest x-rays can detect abnormal symptoms by looking for a number of traits and where they are located. By progressively extracting the most distinguishing features, each CNN layer generates a new representation of the input picture. The initial layer of a network can learn edges and the final layer can detect lung opaqueness; this can be used to categorize COVID-19 and pneumonia, for instance. Retraining the network after deleting the top layer and our selected approach (ii) retraining after removing the n top layers were thus aspects examined in our experimental study. In relation to the used CNNs, the parameter n varies with the overall number of layers in every model framework. Following the selection of the n-threshold, the following model components were "un-frozen" and fine-tuned. We used the first n layers as a predetermined feature extractor and trained the successive layers to recognize particular x-ray features.

Mathematical morphology has been used to enhance contrast in chest x-ray images. The structural qualities of objects are the basis of mathematical morphology methods. These methods isolate specific areas of an image by employing mathematical building blocks and interactions across classes to extract relevant elements. Morphological operators take two datasets as input. The source image is located in the first set, whiles the structural element (SE), sometimes called a mask, is shown in the second set. Binary or greyscale images serve as the basis for the mask, which is a matrix of 0s and 1s values. Equations define the erosion and dilation operators for morphological operators. Given that S(u, v) represents the SE and I(x, y) represents the gray-level image matrix, then

$$I \Theta S = \min\{I(x + u, y + v) - S(u, v)\}$$

$$I \oplus S = \max\{I(x - u, y - v) + S(u, v)\}$$

When an image is eroded, the object size shrinks, the hole size expands, and exceedingly fine details are erased. The final product seems darker than the source because to the removal of intense areas under the SE. Reversing the dilation operator causes things to enlarge while picture holes contract. That is to say, the opening operator is like doing the erosion and dilation processes on the exact image Eq, and the closure operator does the inverse.

$$I \circ S = (I \Theta S) \oplus S$$

$$I \bullet S = (I \oplus S) \Theta S$$

The closing operator addresses minor gaps, while the beginning operator removes negative associations among artifacts and little information. A disk-shaped SE is the most common type of medical image mask, albeit the size and form of SEs are often determined at random.

5. PERFORMANCE RESULTS

In Table 2, you can see a rundown of all the classifier algorithms that were considered for the study, along with their respective efficiency ratings. Some examples of these are True Positive (TP), False Negative (FN), and False Positive (FP). A fundamental metric that generates accurate predictions is known as a true positive (TP), but false positives (FP) show that the inverse is true and that the positive predictions are inaccurate. The accuracy of the

Journal of Information Systems Engineering and Management
2025, 10(37s)
e-ISSN: 2468-4376
https://www.jisem-journal.com/

Research Article

negative predictions is measured by true negatives (TN), whereas false negatives (FN) are the inaccurate predictions. The performance measure formulas are shown in equations (7) and (6). Shown in figure 3.

Table 2. The Confusion Matrix

		Actual Values	
		Positive	Negative
Predicted Values	Positive	TP	FP
	Negative	FN	TN

$$\text{Accuracy}=\frac{(TP+TN)}{(TP+TN+FP+FN)}$$

$$\text{Precision} = \frac{TP}{TP + FP}$$

$$\text{Recall}=\frac{TP}{TP+FN}(10)$$

$$F - Score = \frac{(2 * TP)}{(2 * TP + FP + FN)}$$

One popular performance and probability curve measure is the Area under the Curve (AUC-ROC) for problems with binary classification. The discrimination capability of the classification model is shown in this graph. The ROC curve displays the true positive rate on the y-axis and the false positive rate on the x-axis. The area under the curve (AUC) ranges from 0 to 1. Area under the curve (AUC) models that are close to 1 do exceptionally well in classification tasks; models that are close to 0.5 exhibit absolutely no reparability; and models that are close to 0 do quite badly

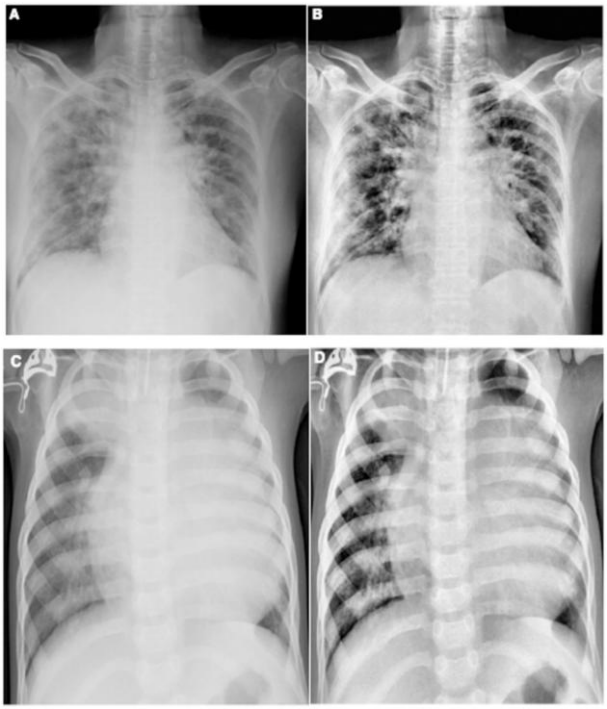

Figure 3 One popular performance and probability curve measure is the Area under the Curve (AUC-ROC) for problems with binary classification.

The discrimination capabilities of the classification model are shown in this graph. The ROC curve displays the true positive rate on the y-axis and the false positive rate on the x-axis. The area under the curve (AUC) ranges from 0 to 1. Area under the curve (AUC) models that are close to 1 do exceptionally well in classification tasks; models that are close to 0.5 exhibit absolutely no reparability; and models that are close to 0 do quite badly.
. The confusion matrix's potential outcomes are valued based on the performance parameters listed below.

Journal of Information Systems Engineering and Management
2025, 10(37s)
e-ISSN: 2468-4376
https://www.jisem-journal.com/

Research Article

Table 3. Matrix relates to confusion based on attribute values.

	Predictive Positive	Predictive Negative	Total
Actual Positive	*TP*	*FN*	*TP + FN*
Actual Negative	*FP*	*TN*	*FP + TN*
Total	*TP + FP*	*FN + TN*	

TP = True Positive, FN = False Negative, FP = False Positive, TN = True Negative.

Accuracy: A crucial parameter for ensuring the performance of DL classifiers is accuracy. It is a breakdown of the all values of the matrix components split by the confusion of the true positives and true negatives. Representation of visual feature of covid 19 bio-medical human images shown in figure 4.

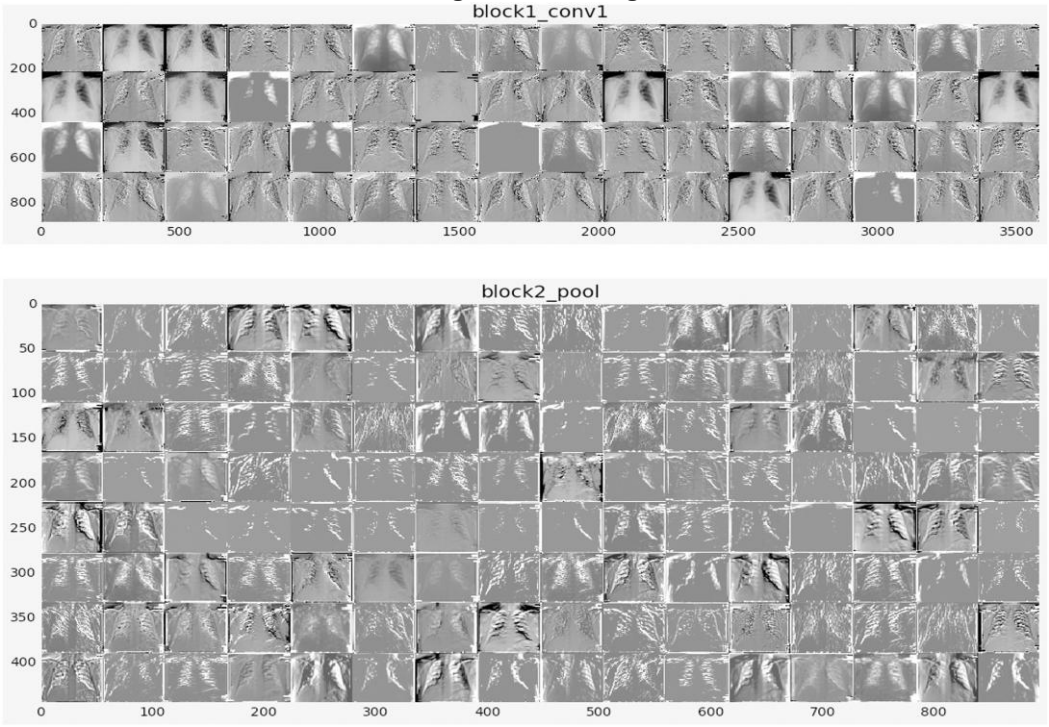

Figure 4 Layer by Layer visual feature extractions from medical human covid images.

When testing on symmetric data sets, the optimal and most accurate model will have approximately similar false positive and false negative values. We will calculate the elements of the confusion matrix to see how well our projected classification model works with the COVID-19 database.

5.1. DISCUSSIONS AND OUTCOMES

This work's simulation study was carried out using the Python platform. For the data classification, we utilized RF, ARF, and SVM. Only 25% (48 observations) of the total data was utilized for classifier testing, whereas 75% (147 observations) went into model training. To ensure the system accurately identified CD symptoms, a ten-fold cross validation technique be used.

Synopsis of the collected data

The credit for the collection of Covid data has gone to the UCI Repository [5]. In the database, you may find 756 samples. One of its 754 unique attributes is the Class label attribute. The data for the study came from 188 CD patients, 107 of whom were male and 81 of whom were female, with ages varied between 33 to 87. These patients got treatment at the Department of Neurology at the Cerrahpaşa Faculty of Medicine, Istanbul University. There are 64 healthy individuals that participated in the control group; the ages of the participants range from 41 to 82. There are 23 men and 41 women in the group. Examining the effects of various feature ranking algorithms on this dataset is the major objective of this study. Our three feature rating strategies are detailed in the recommended section of this inquiry

The feature rankings for each rating technique are as follows:

Journal of Information Systems Engineering and Management
2025, 10(37s)
e-ISSN: 2468-4376
https://www.jisem-journal.com/

Research Article

Rank	Gain Ratio	Score	Information Gain	Score	Improved Correlation	Score
1	MDVP.FloHz	0.3941	PPE	18.1976	Spread1	0.1636
2	Spread1	0.2190	MDVP.FloHz	17.3215	PPE	0.1564
3	MDVP.APQ	0.2157	Spread1	16.2466	Spread2	0.1362
4	PPE	0.2108	Spread2	12.2796	DFA	0.1056
5	NHR	0.1977	MDVP.FhiHz	11.3707	RCDE	0.0991
6	Spread2	0.1952	MDVP.FloHz	10.8613	MDVP.FoHz	0.0964
7	MDVP.FhiHz	0.1915	MDVP.APQ	9.4973	MDVP.FloHz	0.0924
8	MDVP.RAP	0.1881	RCDE	8.9384	HNR	0.0889
9	Jitter.DDP	0.1882	MDVP.Shimmer	8.6974	Shimmer.APQ3	0.0809
10	MDVP.Shimmer	0.1879	MDVP.JitterAbs	8.5995	Shimmer. DDA	0.0807
11	Shimmer.APQ5	0.1829	Shimmer.APQ5	8.3034	MDVP.Shimmer	0.0781
12	MDVP.ShimmerdB	0.1754	Shimmer.APQ3	8.2813	Shimmer.APQ5	0.0744
13	MDVP.FoHz	0.1676	HNR	8.2652	MDVP.PPQ	0.0703
14	Shimmer.APQ3	0.1619	MDVP.RAP	8.0834	MDVP.JitterAbs	0.0671
15	Shimmer.DDA	0.1607	Shimmer.DDA	8.0419	MDVP.RAP	0.0619
16	MDVP.JitterAbs	0.1595	Jitter.DDP	8.0006	Jitter.DDP	0.0619
17	MDVP.PPQ	0.1566	DFA	7.7938	MDVP.ShimmerdB	0.0616
18	MDVP.Jitter	0.1485	MDVP.ShimmerdB	7.7232	MDVP.Jitter	0.0609
19	HNR	0.1099	D2	7.2963	MDVP.APQ	0.0543
20	RCDE	0.0845	MDVP.PPQ	6.9608	MDVP.FhiHz	0.0448
21	D2	0.0784	MDVP.Jitter	6.8061	D2	0.0405
22	DFA	0.0724	NHR	6.5259	NHR	0.0265

Table 4. Feature Ranking results for each ranking technique

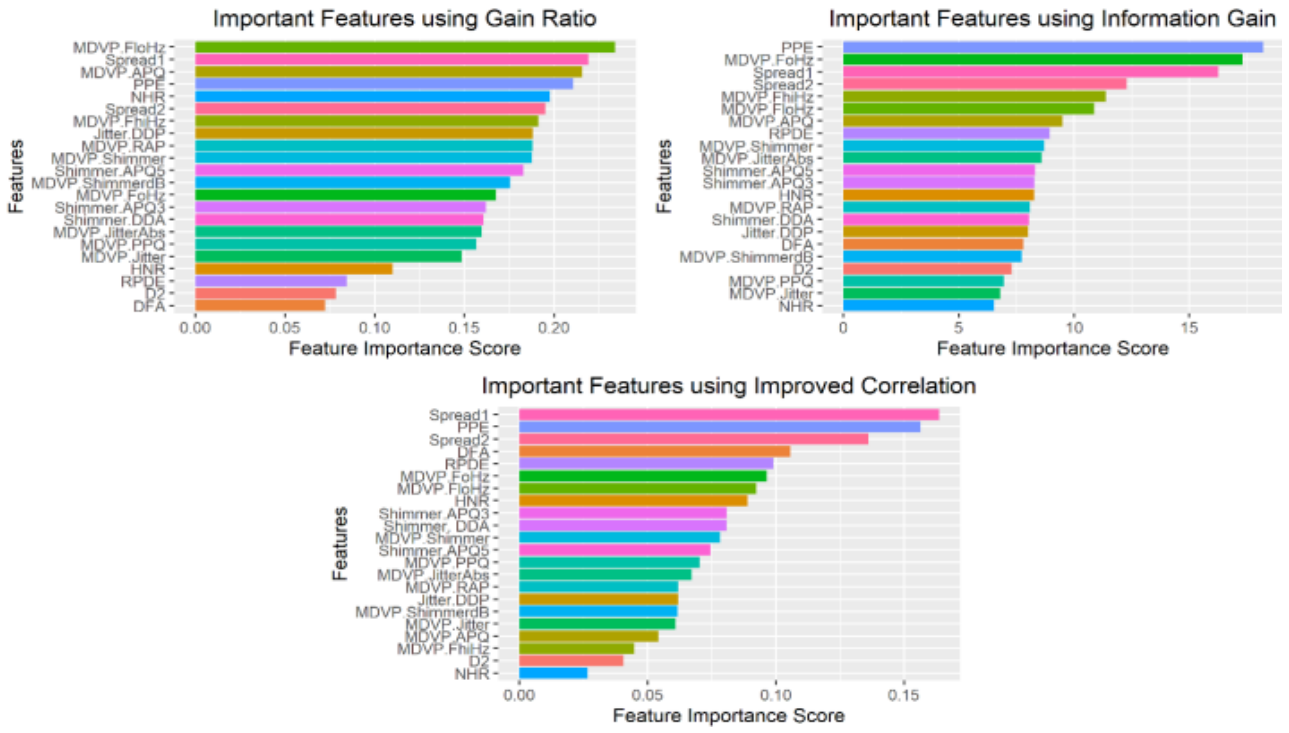

Figure 5 the results of the feature rating for each ranking approach.

Each classifier in the experiment underwent a 10-fold cross validation.

Journal of Information Systems Engineering and Management
2025, 10(37s)
e-ISSN: 2468-4376
https://www.jisem-journal.com/

Research Article

F-score, recall, precision, and accuracy were used to gauge a classifier's effectiveness. The trial results for various machine learning methods, with or without feature selection approaches, are exposed in Table-5

Table 5. Performance of the Classifier Before and After Feature Selection

Performance Classifier	**Accuracy**	**Precision**	**Recall**	**F-Score**
Support Vector Machine	0.700	0.701	0.700	0.700
Random Forest	0.738	0.738	0.738	0.737
Adaptive Random Forest	**0.804**	0.807	0.804	0.804

Table.6. Classifier Performance with Features Chosen by Gain Ratio

Performance Classifier	Accuracy	Precision	Recall	F-Score
Support Vector Machine	0.717	0.718	0.717	0.716
Random Forest	0.800	0.802	0.801	0.809
Adaptive Random Forest	**0.829**	0.830	0.829	0.829

Table.7. Classifier Performance with Features Chosen according to Information Gain

Performance Classifier	**Accuracy**	**Precision**	**Recall**	**F-Score**
Support Vector Machine	0.779	0.781	0.779	0.779
Random Forest	0.817	0.820	0.817	0.816
Adaptive Random Forest	**0.838**	0.839	0.838	0.837

Table 8. Performance Evaluation of Classifiers with Feature Selection Based on Enhanced Correlation

Performance Classifier	**Accuracy**	**Precision**	**Recall**	**F-Score**
Support Vector Machine	0.804	0.806	0.804	0.804
Random Forest	0.846	0.848	0.846	0.846
Adaptive Random Forest	**0.883**	0.884	0.883	0.883

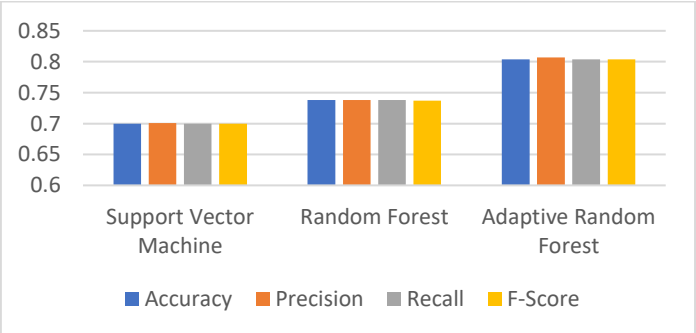

Figure 6: Evaluating Classifier Performance Ignoring Feature Selection

Journal of Information Systems Engineering and Management
2025, 10(37s)
e-ISSN: 2468-4376
https://www.jisem-journal.com/

Research Article

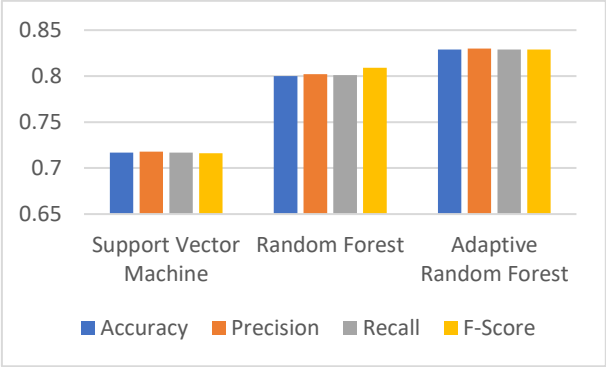

Figure 7: Assessing Classifier Performance using Gain Ratio-Based Feature Selection

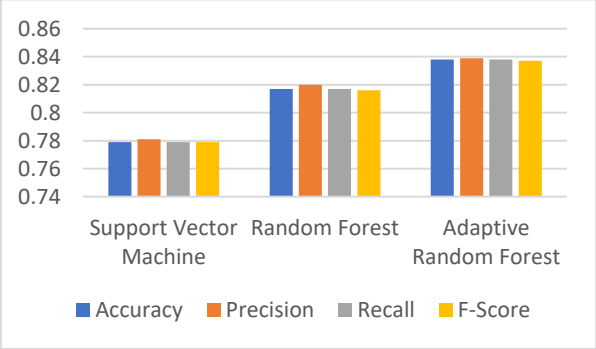

Fig. 8. Classifier Performance Evaluation Using Information Gain-Based Feature Selection

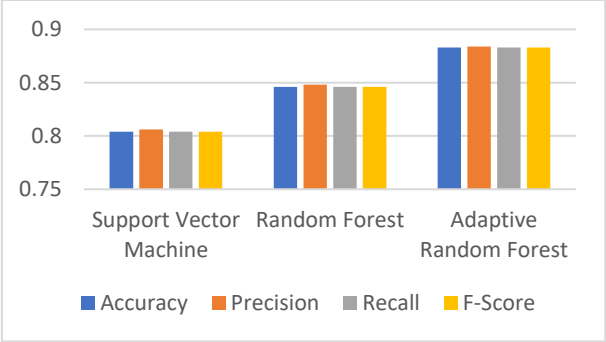

Figure 9: Classifier Performance Evaluation Using Enhanced Correlation-Based Feature Selection

5.2. Confusion Matrix

As such, the confusion matrix and additional measures of classification performance for numerous techniques on the Covid data set are exposed in the table that follows. The precision, recall, F1-Score, and true positive/true negative matrix, as well as the support and recall metrics, were derived from the modules that were put into practice. The final precision was determined by applying these standards

Table 9. Perplexity Matrix for Various Algorithms

<table>
<tr><th>S.No</th><th>Algorithm</th><th>Confusion Matrix</th></tr>
<tr><td>1</td><td>SVM</td><td>
<table>
<tr><th colspan="2" rowspan="2">Predicated Values</th></tr>
<tr></tr>
<tr><th rowspan="3">Actual Values</th><td></td><td>Positive</td><td>Negative</td></tr>
<tr><td>Positive</td><td>108</td><td>08</td></tr>
<tr><td>Negative</td><td>12</td><td>24</td></tr>
</table>
</td></tr>
<tr><td>2</td><td>RF</td><td>
<table>
<tr><th colspan="2" rowspan="2">Predicated Values</th></tr>
<tr></tr>
<tr><th rowspan="3">Actual Values</th><td></td><td>Positive</td><td>Negative</td></tr>
<tr><td>Positive</td><td>93</td><td>22</td></tr>
</table>
</td></tr>
</table>

Journal of Information Systems Engineering and Management
2025, 10(37s)
e-ISSN: 2468-4376
https://www.jisem-journal.com/

Research Article

			Negative	12	25
3	ARF	**Predicated Values**			
		Actual Values		Positive	Negative
			Positive	107	03
			Negative	30	12

Table 10. Performance Measures for the Three Methods Employing the Ensemble Approach

S.No	Algorithm	Metrics				
1	SVM		Precision	Recall	F1_Score	Accuracy
		Abnormal	0.76	0.68	0.72	78.34%
		Healthy	0.91	0.94	0.92	
		Avg	0.84	0.81	0.82	
2	RF		Precision	Recall	F1_Score	Accuracy
		Abnormal	0.54	0.69	0.61	82.37%
		Healthy	0.89	0.82	0.86	
		Avg	0.82	0.79	0.79	
3	ARF		Precision	Recall	F1_Score	Accuracy
		Abnormal	0.81	0.32	0.43	84.54%
		Healthy	0.79	0.98	0.88	
		Avg	0.81	0.78	0.74	

The Random Forest algorithm offers the best accuracy, at 82.37%, closely followed by the Adaptive Random Forest approach at 84.54%, according to the conclusions derived from the data. Ultimately, these algorithms can help predict if an individual will get CD.

5.3. ROC AnalysisCovid's Disease Data

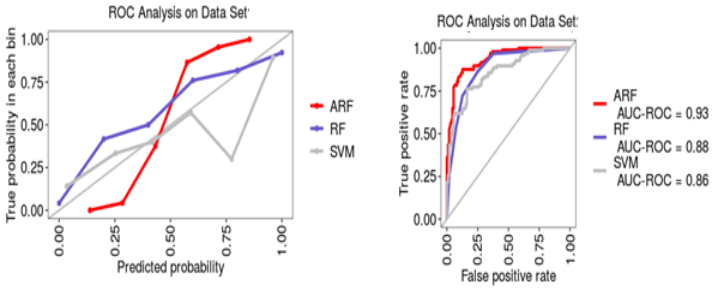

Fig. 10: The Adaptive Random Forest Classifier Was Analyzed Using Covid's Disease Data.

Figure 10 shows that compared to RF (88%), SVM (86%), and the proposed classification approach employing the suggested feature selection method (93%) on the Covid's Disease Data set, the AUC-ROC values were much higher for the latter two.

6. CONCLUSION

To maximize feature selection efficiency and give the classifier its best performance. In this paper, we develop a new system for autonomously diagnosing COVID-19 sickness with data from chest X-ray and CT scans. The system is a stacked convolutional neural network. Instead of using an existing model that has already been trained, the proposed method trains a new model from scratch using a deep learning architecture—more particularly, a CNN architecture—and does away with the requirement for manual feature extraction. Using a publicly accessible chest X-ray radiograph dataset, the entire experimental study was performed. This study's output is a suggested model with a 98.33% accuracy rate. Additionally, the suggested scheme has been validated by considering several hyperparameters, and a number of comparisons were examined by taking into account of four pre-trained transfer

learning systems in addition to current cutting-edge methodologies. The suggested method produces improved results in every area of experimental analysis for COVID-19 infection detection. This suggested device can help radiologists identify COVID-19 patients early and reduce diagnostic error because it is lightweight, more durable, and ideal for use.

REFERENCES

[1] Wang, W., Xu, Y., Gao, R., Lu, R., Han, K., Wu, G., & Tan, W. (2020). Detection of SARS-CoV-2 in Different Types of Clinical Specimens. JAMA, 323(18), 1843–1844. https://doi.org/10.1001/jama.2020.3786

[2] Sitaula, C., Aryal, S. New bag of deep visual words based features to classify chest x-ray images for COVID-19 diagnosis. Health Inf Sci Syst 9, 24 (2021). https://doi.org/10.1007/s13755-021-00152-w

[3] Liu, Y., Whitfield, C., Zhang, T. et al. Monitoring COVID-19 pandemic through the lens of social media using natural language processing and machine learning. Health Inf Sci Syst 9, 25 (2021). https://doi.org/10.1007/s13755-021-00158-4

[4] Guan WJ, Ni ZY, Hu Y, et al. Clinical Characteristics of Coronavirus Disease 2019 in China. N Engl J Med. 2020;382(18):1708-1720. doi:10.1056/NEJMoa2002032

[5] Narin, A., Kaya, C. & Pamuk, Z. Automatic detection of coronavirus disease (COVID-19) using X-ray images and deep convolutional neural networks. Pattern Anal Applic 24, 1207–1220 (2021). https://doi.org/10.1007/s10044-021-00984-y

[6] Wang, L., Lin, Z.Q. & Wong, A. COVID-Net: a tailored deep convolutional neural network design for detection of COVID-19 cases from chest X-ray images. Sci Rep 10, 19549 (2020). https://doi.org/10.1038/s41598-020-76550-z

[7] Ozturk, Tulin et al. “Automated detection of COVID-19 cases using deep neural networks with X-ray images.” Computers in biology and medicine vol. 121 (2020): 103792. doi:10.1016/j.compbiomed.2020.103792

[8] Supriya, Supriya et al. “Automated epilepsy detection techniques from electroencephalogram signals: a review study.” Health information science and systems vol. 8,1 33. 12 Oct. 2020, doi:10.1007/s13755-020-00129-1

[9] Sarki, Rubina et al. “Automated detection of mild and multi-class diabetic eye diseases using deep learning.” Health information science and systems vol. 8,1 32. 8 Oct. 2020, doi:10.1007/s13755-020-00125-5

[10] R. Sarki, K. Ahmed, H. Wang and Y. Zhang, "Automatic Detection of Diabetic Eye Disease Through Deep Learning Using Fundus Images: A Survey," in *IEEE Access*, vol. 8, pp. 151133-151149, 2020, doi: 10.1109/ACCESS.2020.3015258

[11] Li, X., Zhou, Y., Du, P. et al. A deep learning system that generates quantitative CT reports for diagnosing pulmonary Tuberculosis. Appl Intell 51, 4082–4093 (2021). https://doi.org/10.1007/s10489-020-02051-1

[12] Ng, Ming-Yen et al. “Imaging Profile of the COVID-19 Infection: Radiologic Findings and Literature Review.” Radiology. Cardiothoracic imaging vol. 2,1 e200034. 13 Feb. 2020, doi:10.1148/ryct.2020200034

[13] Cohen JP, Morrison P, Dao L. COVID-19 image data collection. arXiv 200311597. 2020;.

[14] Li X, Zhu D. Covid-xpert: An ai powered population screening of covid-19 cases using chest radiographyimages. arXiv preprint arXiv:200403042. 2020;.

[15] Shervin Minaee, Rahele Kafieh, Milan Sonka, Shakib Yazdani, Ghazaleh Jamalipour Soufi,Deep-COVID: Predicting COVID-19 from chest X-ray images using deep transfer learning,Medical Image Analysis,Volume 65,2020,101794,ISSN 1361-8415,https://doi.org/10.1016/j.media.2020.101794

[16] Sarki, Rubina et al. “Automated detection of COVID-19 through convolutional neural network using chest x-ray images.” PloS one vol. 17,1 e0262052. 21 Jan. 2022, doi:10.1371/journal.pone.0262052

[17] H. Nasiri a, *, S. Hasani, "Automated detection of COVID-19 cases from chest X-ray images usingdeep neural network and XGBoost", Radiography 28 (2022) 732e738

[18] Wu F, Zhao S, Yu B, Chen Y, Wang W, Song Z, et al. A new coronavirus associatedwith human respiratory disease in China. Nature 2020;579:265e9.

[19] Sohrabi C, Alsafi Z, O’neill N, Khan M, Kerwan A, Al-Jabir A, et al. World HealthOrganization declares global emergency: a review of the 2019 novel coronavirus(COVID-19). Int J Surg 2020;76:71e6.

[20] Jha N, Prashar D, Rashid M, Shafiq M, Khan R, Pruncu C, et al. Deep learningapproach for discovery of in silico drugs for combating COVID-19. J HealthcEng2021:2021.

[21] Wu Z, McGoogan JM. Characteristics of and important lessons from the coronavirusdisease 2019 (COVID-19) outbreak in China: summary of a report of 72314 cases from the Chinese Center for Disease Control and Prevention. JAMA2020;323:1239e42.

[22] Huang P, Liu T, Huang L, Liu H, Lei M, Xu W, et al. Use of chest CT in combinationwith negative RT-PCR assay for the 2019 novel coronavirus but highclinical suspicion. Radiology 2020;295:22e3.

[23] Ng MY, Lee EY, Yang J, Yang F, Li X, Wang H, et al. Imaging profile of the COVID-19 infection: radiologic findings and literature review. RadiolCardiothoracImag2020;2:e200034.

[24] Liu H, Liu F, Li J, Zhang T, Wang D, Lan W. Clinical and CT imaging features ofthe COVID-19 pneumonia: focus on pregnant women and children. J Infect2020;80:e7e13.

[25] Chen N, Zhou M, Dong X, Qu J, Gong F, Han Y, et al. Epidemiological and clinicalcharacteristics of 99 cases of 2019 novel coronavirus pneumonia in Wuhan,China: a descriptive study. Lancet 2020;395:507e13.

[26] Ozturk T, Talo M, Yildirim EA, Baloglu UB, Yildirim O, Acharya UR. Automateddetection of COVID-19 cases using deep neural networks with X-ray images.ComputBiol Med 2020;121:103792.

[27] Tian X, Wang J, Du D, Li S, Han C, Zhu G, et al. Medical imaging and diagnosis ofsubpatellar vertebrae based on improved Laplacian image enhancement algorithm.Comput Methods Progr Biomed 2020;187:105082.

[28] Hannan R, Free M, Arora V, Harle R, Harvie P. Accuracy of computer navigationin total knee arthroplasty: a prospective computed tomography-based study.Med Eng Phys 2020;79:52e9.

[29] Liang C, Liu Y, Wu M, Garcia-Castro F, Alberich-Bayarri A, Wu F. Identifyingpulmonary nodules or masses on chest radiography using deep learning:external validation and strategies to improve clinical practice. ClinRadiol2020;75:38e45.

[30] Hussein S, Kandel P, Bolan CW, Wallace MB, Bagci U. Lung and pancreatic tumorcharacterization in the deep learning era: novel supervised and unsupervisedlearning approaches. IEEE Trans Med Imag2019;38:1777e87.

[31] Mahesh Goura,*, Sweta Jain a, "Automated COVID-19 detection from X-ray and CTimages with stacked ensemble convolutionalneural network", biocybernetics and biomedical engineering 42 (2022) 27– 41.

[32] Shi F,Wang J, Shi J,WuZ,Wang Q, Tang Z, He K, Shi Y, Shen D.Review of artificial intelligence techniques in imaging dataacquisition, segmentation, and diagnosis for covid-19. IEEERev Biomed Eng 2021;14:4–15. https://doi.org/10.1109/RBME.2020.2987975.

[33] Dong D, Tang Z, Wang S, Hui H, Gong L, Lu Y, Xue Z, Liao H,Chen F, Yang F, et al. The role of imaging in the detection andmanagement of covid-19: A review. IEEE Rev Biomed Eng2021;14:16–29. https://doi.org/10.1109/RBME.2020.2990959.

[34] Xu, Xiaowei et al. “A Deep Learning System to Screen Novel Coronavirus Disease 2019 Pneumonia.” Engineering (Beijing, China) vol. 6,10 (2020): 1122-1129. doi:10.1016/j.eng.2020.04.010

[35] Shah V, Keniya R, Shridharani A, Punjabi M, Shah J,Mehendale N. Diagnosis of covid-19 using ct scan images anddeep learning techniques. Emergency Radiol2021;28:497–505.https://doi.org/10.1007/s10140-020-01886-y.

[36] Kassania, Sara Hosseinzadeh et al. “Automatic Detection of Coronavirus Disease (COVID-19) in X-ray and CT Images: A Machine Learning Based Approach.” Biocybernetics and biomedical engineering vol. 41,3 (2021): 867-879. doi:10.1016/j.bbe.2021.05.013

[37] Wang J, BaoY,Wen Y, Lu H, Luo H, Xiang Y, Li X, Liu C, Qian D.Prior-attention residual learning for more discriminativecovid-19 screening in ct images. IEEE Trans Med Imaging2020;39(8):2572–83. https://doi.org/10.1109/TMI.2020.2994908.

[38] Afshar P, Heidarian S, Naderkhani F, Oikonomou A,Plataniotis KN, Mohammadi A. Covid-caps: A capsulenetwork-based framework for identification of covid-19 casesfrom x-ray images. Pattern Recogn Lett 2020;138:638–43.https://doi.org/10.1016/j.patrec.2020.09.010.

[39] Ardakani AA, Kanafi AR, Acharya UR, Khadem N,Mohammadi A. Application of deep learning technique tomanage covid-19 in routine clinical practice using ct images:Results of 10 convolutional neural networks.

Research Article

ComputBiolMed 2020;121 . https://doi.org/10.1016/j.compbiomed.2020.103795 103795.

[40] Mishra NK, Singh P, Joshi SD. Automated detection of covid-19 from ct scan using convolutional neural network.Biocybernetics Biomed Eng 2021;41(2):572–88. https://doi.org/10.1016/j.bbe.2021.04.006.

[41] A. Narin, C. Kaya, Z. Pamuk, Automatic detection ofcoronavirus disease (covid-19) using x-ray images and deepconvolutional neural networks, Pattern Analysis andApplications doi: 10.1007/s10044-021-00984-y.

[42] Oh Y, Park S, Ye JC. Deep learning covid-19 features on cxrusing limited training data sets. IEEE Trans Med Imaging2020;39(8):2688–700. https://doi.org/10.1109/TMI.2020.2993291.

[43] Ozturk, Tulin et al. "Automated detection of COVID-19 cases using deep neural networks with X-ray images." Computers in biology and medicine vol. 121 (2020): 103792. doi:10.1016/j.compbiomed.2020.103792

[44] Rodolfo M. Pereira, Diego Bertolini and Lucas O. Teixeira et al. COVID-19 identification in chest X-ray images on flat and hierarchical classification scenarios. Comput Methods Programs Biomed. 2020. DOI: 10.1016/j.cmpb.2020.105532

[45] P.K. Sethy, S.K. Behera, P.K. Ratha, P. Biswas, Detection ofcoronavirus disease (covid-19) based on deep features andsupport vector machine, Preprints 2020030300.

[46] Minaee, Shervin et al. "Deep-COVID: Predicting COVID-19 from chest X-ray images using deep transfer learning." Medical image analysis vol. 65 (2020): 101794. doi:10.1016/j.media.2020.101794

[47]Isabella Castiglioni, Davide Ippolito, Matteo Interlenghi, Caterina
Beatrice Monti, Christian Salvatore, Simone Schiaffino, Annalisa Polidori, Davide Gandola, Cristina Messa, Fran cesco Sardanelli, Artificial intelligence applied on chest x-ray can aid in the diagnosis of covid-19 infection: a first experiencefrom lombardy, italy, medRxiv 2020.04.08.20040907; doi: https://doi.org/10.1101/2020.04.08.20040907

[48] Abraham, Bejoy, and Madhu S Nair. "Computer-aided detection of COVID-19 from X-ray images using multi-CNN and Bayesnet classifier." Biocybernetics and biomedical engineering vol. 40,4 (2020): 1436-1445. doi:10.1016/j.bbe.2020.08.005